Hierarchical Electrode Design of Highly Efficient and Stable Unitized Regenerative Fuel Cells (URFCs) for Long-term Energy Storage

Xiong Peng[1], Zachary Taie[1,2], Jiangjin Liu[1], Yaqian Zhang[3,4], Xinxing Peng[3], Yagya N. Regmi[1], Julie C. Fornaciari[1,5], Christopher Capuano[6], Dustin Binny[7], Nancy N. Kariuki[8], Deborah J. Myers[8], Mary C. Scott[3,4], Adam Z. Weber[1], Nemanja Danilovic[1,*]

[1] Energy Storage and Distributed Resources Division, Lawrence Berkeley National Laboratory, Berkeley, CA, 94720, USA

[2] Oregon State University, School of Mechanical, Industrial, and Manufacturing Engineering, Bend, OR, 97701, USA

[3] National Center for Electron Microscopy, Molecular Foundry, Lawrence Berkeley National Laboratory, Berkeley, CA, 94720, USA

[4] Departments of Materials Science and Engineering, University of California Berkeley, Berkeley, CA, 94720, USA

[5] Departments of Chemical Engineering, University of California Berkeley, Berkeley, CA, 94720, USA

[6] Nel Hydrogen/Proton Onsite, Wallingford, CT, 06492, USA

[7] Ballard Power Systems, Burnaby, British Columbia, V3N 5G2, Canada

[8] Chemical Sciences and Engineering Division, Argonne National Laboratory, Lemont, IL, 60439, USA

* Corresponding author: ndanilovic@lbl.gov

Experimental Sections

Membrane treatment. The Nafion™ perfluorosulfonic acid membranes (N212, Ion Power) were prepared by soaking in DI water at 90 °C for one hour and followed by immersion in 0.5 M HNO_3 (ACS Reagent, Sigma-Aldrich) for one hour at room temperature to remove impurities and protonate the sulfonic-acid groups. Finally, the treated membranes were rinsed three times using DI water to remove excess acid and stored in DI water until catalyst coating is performed.

Catalyst Layer Preparation Using Spray Coating. In this work, for the Pt/C inks, weighted Pt/C (45.6 wt% Pt, Tanaka), water (18.2 MΩ, Milli-Q), 1-propanol (NPA, HPLC grade, Sigma-Aldrich), and Nafion™ (D521, 1100EW, Ion Power) are added into a centrifuge tube in the stated sequence. The ionomer to carbon ratio was maintained at 0.6 for the Pt/C catalyst layer. The ink was sonicated in a bath sonicator (M1800, Branson) equipped with a chiller (Grant) at 10°C for 30 minutes for before spraying. For the unsupported Pt black (TEC90300, Tanaka) and Ir black (SA=100, Tanaka) ink, Pt:Ir (50:50 in weight), water, ethanol (200 proof, Koptec), NPA, and Nafion™ ionomer (D521, 1100 EW, Ion Power) are added into a centrifuge tube as the stated sequence followed by shaken for a minute to ensure well mixing. The ionomer to catalyst (Ir and Pt) ratio was kept at 0.116 for unsupported catalyst layer. The centrifuge tube was hand shaken for one minute then placed in an ice bath ensuring that the entire volume of the ink is submersed in ice water. Using a horn sonicator, the tip of the probe (CEX500, Cole-Parmer) was placed 2 cm from the bottom of the vial and then the top of the vial was covered with Parafilm to avoid solvent evaporation during probe sonication. The ink

was dispensed using a sprayer (SonoTek) with ultrasonic nozzle at rate of 0.2 L min^{-1}. After spraying, the precious metal loading of Pt-Ir bifunctional electrode and Pt/C electrode were measured to be around 1.0 mg cm^{-2} and 0.3 mg cm^{-2} using X-ray fluorescence (XRF) (Bruker).

Catalyst Layer Preparation Using Dr. Blading Technique. The doctor blading process requires more viscous ink. Therefore, a different ink recipe was used. In a small centrifuge tube (10 mL), the Pt black and Ir black catalyst (50:50) was weighted in. After that, the catalyst was moistened using DI water to prevent solvent oxidation. Nafion™ dispersion (D521, EW-1100) was added in so that the ionomer to catalyst ratio was maintained at 0.116. To obtain a homogeneous dispersion, the ink was horn sonicated in ice bath for 30 min before Dr. blading. During the blading process, the membrane is fixed through vacuum on a heated aluminum plate at temperature of 45 °C. A non-permeable gasket was used to mask the membrane and control the electrode active area to be 5 cm^2. A zero gap in-house made doctor blade was used during the blading process. The precious metal loading was measured using XRF (Bruker) after formation of catalyst layer. 25 cm^2 CCMs were also prepared similarly for larger scale testing. After doctor blading, the precious metal loading of Pt-Ir bifunctional electrode and Pt/C electrode were measured to be around 1.0 mg cm^{-2} and 0.3 mg cm^{-2} using X-ray fluorescence (XRF) (Bruker).

Focused ion beam-scanning electron microscope (FIB-SEM) measurements: Cross-sectional SEM images showing serial sections of porous catalysts were obtained by cutting the sample every 20 nm using an FEI Helios G4 dual-beam FIB system equipped

with a Ga^+ ion beam. Three-dimensional structures of porous catalyst layer were reconstructed by stacking the serial-sectioning SEM image using ImageJ software. The pore and solid regions of each serial SEM image set was classified using the Trainable Weka Segmentation plugin in ImageJ.[1] After the segmentation was completed, the 3-dimensional images were reconstructed and rendered using Dragonfly v3.6 (Dragonfly 3.6 [Computer software]). Object Research Systems (ORS) Inc, Montreal, Canada, 2018; software available at http://www.theobjects.com/dragonfly). The porosity, pore connectivity, pore distribution information, and fluid transport parameters were calculated using the OpenPNM package integrated into Dragonfly v3.6.[2] The tortuosity factor was calculated using the TouFactor MATLAB plugin.[3]

Cell Assembly. URFC MEAs with 5 cm^2 active area were assembled in single cell hardware (Fuel Cell Technology) with serpentine flow field on both sides. The CCM was rehydrated at room temperature in DI water before it was assembled into the cell. Teflon gaskets were used on anode and cathode, respectively. Carbon paper with microporous layer (MPL) (Sigracet 29 BC) was used as GDLs. Platinized sintered titanium (obtained from Proton OnSite/NEL) was used as anode porous-transport layers (PTLs) under electrolyzer mode. The appropriate thickness PTFE (McMaster-Carr) gaskets were used in order to obtain 20% compression in GDLs, while thickness-matched gasket were used for the Ti-PTL. For the URFC tests, the Ti-PTL was wet-proofed with PTFE dispersion (DISP 30, Ion Power) according to the procedure described by Ito et. al.[4] The PTFE was maintained as 5% in weight to the PTL.

Cell Testing. A multichannel potentiostat (VSP300, Biologic) equipped with electrochemical impedance spectroscopy (EIS) and a 20A booster was used for all electrochemical tests for both constant-electrode (CE) and constant-gas (CG) modes URFC. The test station used is a modified Fuel Cell Technology (FCT) test stand; the modification is an addition of a water recirculation system for the electrolyzer mode testing. Before any electrochemical testing, a break-in process was performed by holding cell voltage at 0.1 V in fuel cell mode overnight to activate electrodes and purge electrolyte impurities. Polarization curves and electrochemical impedance were first recorded in fuel cell mode, with H_2 and air (or O_2) at flow rate of 300 mL min^{-1} and 750 mL min^{-1} supplied to anode and cathode, respectively. Backpressure was kept at 21 psi for each side. For switching from fuel cell (discharge) to electrolyzer (charge): H_2/Air (O_2) supply was stopped, if it was under CE-URFC mode, N_2 was used to purge at 300 mL min^{-1} on both sides for 5 min; if it was under CG-URFC mode, no N_2 was needed to purge both sides. After that, DI water at 80 °C was supplied on the anode side for electrolyzer operation while 100 mL min^{-1} of H_2 was supplied at cathode at ambient pressure to ensure a pseudo-steady reference electrode for electrolyzer operation. A cyclic voltammetry (CV) conditioning step was then performed by scanning between 0 and 2 V at 50 mV s^{-1} for five cycles before recording polarization curves and electrochemical impedance. The impedance was measured in a galvanostatic mode by applying an AC current perturbation between 200 kHz – 100 mHz to the cell and measuring its voltage response at each polarization step. The amplitude of the AC current was chosen for each step to obtain a sufficient signal to noise ratio, while keeping the perturbation small enough to ensure a linear system response. For switching from

electrolyzer (charge) to fuel cell (discharge): DI supplied was stopped, if it was under CE-URFC mode, N_2 was used to purge at 300 mL min^{-1} on both sides for 5 min; if it was under CG-URFC mode, no N_2 was needed to purge both sides. After that, H_2 and Air(O_2) was supplied to each side of the cell for fuel cell mode operation.

For performance and longevity testing: In CE mode, tests were conducted in a 5 cm^2 URFC device at 1 A cm^{-2} during both charge and discharge. CG mode longevity test was conducted in a 5 cm^2 URFC device at 1 A cm^{-2} and 0.5 A cm^{-2} for charge and discharge, respectively. Identical conditions were used as those described above for polarization curve measurements.

Half-cell testing: Electrochemical measurements were conducted on a thin film rotating disk electrode (RDE) in a three-electrode glass cell using a platinum mesh as the counter electrode and Ag/AgSO$_4$ as the reference electrode. The working electrode was prepared on a 6 mm glassy carbon disk electrode (Pine Research Instrumentation) by dropping 7.5 μL of a catalyst ink with the following composition: 7.6 mg catalyst, 7.6 mL IPA, 2.4 mL DI water and 20 μL 5% Nafion dispersion, and drying on an inverted rotator at 700 RPM at room temperature. The Pt black loading was kept around 20 μg/cm^2. The three-electrode cell was washed using 18.2 MΩ Millipore DI water and 0.1M HClO$_4$ five times each before testing. All the tests were conducted in 0.1M HClO$_4$ electrolyte at room temperature and ambient pressure.

The accelerated stress test (AST) was conducted by cycling the working electrode between 0.06 V and 1.63 V (vs. RHE), which was the typical working potential of the CE-URFC anode. The scanning rate was 10 mV/s. At different cycling stages (0 cycle, 100 cycles, 1000 cycles, 2500 cycles and 5000 cycles), hydrogen oxidation reaction

polarization curves were taken by scanning the working electrode from 0 V to 0.4 V (vs. RHE) at 10 mV/s. The working electrode was rotating at 1600 rpm and hydrogen gas was purged to the electrolyte during the whole test.

Another separate test was conducted using Ir black as catalyst. The sample preparation and AST conditions were the same as the Pt black, except the polarization curve was taken for oxygen evolution reaction by scanning the working electrode from 1.05 V to 1.60 V at 10 mV/s. The working electrode was rotating at 1600 rpm and oxygen gas was purged to the electrolyte during the whole test.

X-ray Scattering: The X-ray scattering data were collected on a combined Bonse−Hart (USAXS) and pinhole (small angle and wide angle X-ray scattering, SAXS/WAXS) instrument at beamline 9-ID-C at the Advanced Photon Source located at Argonne National Laboratory. Details regarding the optics and instrumentation have been previously reported.[5–8] The X-ray beam was monochromatized via a pair of Si(220) crystals to an energy of 21 keV. The beam spot size for USAXS was 0.8×0.6 mm (horizontal $\times$ vertical) and 0.8×0.2 mm for SAXS and WAXS. The data acquisition times were 90 s for USAXS and 30 s for both SAXS and WAXS. The samples were prepared by transferring the electrode layers from their respective substrates to single-sided, transparent 3M Scotch Magic tape using a press-peel technique. The samples were then supported in a custom-made sample holder for the WAXS/SAXS/USAXS measurements. During data reduction, patterns collected on a blank piece of tape were subtracted from the patterns acquired for the samples. The data were background corrected and reduced with the NIKA software package, and data analysis was conducted

using the IRENA software package.[8] Both packages were run on IGOR Pro 8.0 (Wavemetrics). Particle size distribution was obtained from the measured scattering data using the maximum entropy (MaxEnt) method,[5] which involves a constrained optimization of parameters to solve the scattering equation:

$$I(q) = \Delta Q|2\int |F(q, r)|2(V(r))2Np\ (r)dr$$

Where, I(q) is the scattered intensity, Q is the scattering length density of the particle, and F(q, r) is the scattering function at scattering vector q of a particle of characteristic dimension r, V is the volume of the particle, and Np is the number density of particles in the scattering volume.

Round trip efficiency calculation: The overall reaction is

$$H_2O_{(liquid)} \underset{charge}{\overset{discharge}{\rightleftharpoons}} H_{2(g)} + \tfrac{1}{2}\,O_{2(g)}$$
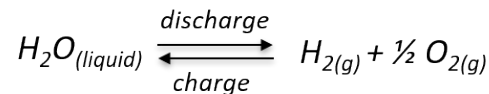
The reversible potential $E_{rev,\,(T,P)}$ is governed by temperature and activity of the species:

$$E_{rev,\,(T,\,P)} = E_{rev}^0 + \frac{RT}{2F}ln[\frac{a(H_2)\cdot\sqrt{a(O_2)}}{a(H_2O)}]$$

At a temperature of 80 °C, the saturation pressure of H_2O is 0.47 bar_a. For liquid water, the activity of water is $a(H_2O)$ is one, while the activity of the gaseous species is represented by the ratio of their partial pressure to the standard pressure of 1 bar. The temperature dependent standard reversible potential, E_{rev}^0, can be obtained from the literature.[9]

$$E_{rev}^0 = 1.2291\ V - 0.0008456\ V\cdot(T - 298.15K)$$

The $E_{rev,\,(T,P)}$ is calculated to be 1.20 V and 1.198 V under O_2 and air fed, respectively.

Therefore, the fuel cell efficiency at each current density is given by:

$$FC_{effi} = \frac{V_{measured}}{E_{rev,(T,P)}} * 100\%$$

Under the electrolyzer testing condition, the $E_{rev,\ (T,P)}$ is calculated to be 1.168 V. Since the energy required for splitting of a mole of liquid water to produce a mole of H_2 at 25 °C is not only from electricity but also heat[10], which adds an additional 0.252 V in addition to the calculated $E_{rev,\ (T,P)}$.

Then, the electrolyzer efficiency at each current density is given by:

$$EC_{effi} = \frac{1.42}{V_{measured}} * 100\%$$

And the related RTE for URFC is give by:

$$RTE = FC_{effi} * EC_{effi}$$

Overpotential analysis. The cell voltage E_{cell} is composed of the sum of the reversible cell potential $E_{(p,T)}^0$ and the three main overpotential η_i:

During charging: $\quad E_{cell} = E_{(P,T)}^0 + \eta_{kin} + \eta_\Omega + \eta_{mt}$

During discharging: $\quad E_{(P,T)}^0 = E_{cell} + \eta_{kin} + \eta_\Omega + \eta_{mt}$

where η_{kin} is the kinetic, η_Ω the ohmic and η_{mt} the mass transport overpotential. For both fuel cell and electrolyzer operation, there are two half reactions happening simultaneously. Since both HOR and HER are more favorable in kinetics and mass transport under current testing conditions compared to ORR and OER, respectively. Therefore, overpotential analysis mainly considers the ORR and OER side.

Ohmic overpotential η_Ω. The EIS is used to measure the high frequency resistance (HFR) representing the total electric cell resistance R_{tot}. The η_Ω is therefore determined as:

$$\eta_\Omega = j * R_{tot} = j * HFR$$

Kinetics overpotential η_{kin}. The kinetic overpotential was extracted using a Tafel model, in which the Tafel slope b and exchange current density j_0 are the governing kinetic parameters. Assuming a non-polarizable HER and HOR reaction, the entire kinetic overpotential of the URFC is governed by OER and ORR with the Tafel slope b as $2.303*RT/nF$:

$$\eta_{kin} = b * log_{10}(\frac{j}{j_0})$$

Mass transport overpotential η_{mt}. The mass transport is a summary of gaseous/liquid transfer in the PTL/CL and ionic transport in the catalyst layers. In this study, it is calculated using the following equation:

During charging: $\quad \eta_{mt} = E_{cell} - E^0_{(P,T)} - \eta_{kin} - \eta_{\Omega}$

During discharging: $\quad \eta_{mt} = E^0_{(P,T)} - E_{cell} - \eta_{kin} - \eta_{\Omega}$

Mathematical modeling: The 2D 2-phase cross-sectional continuum fuel cell model was first developed by Balliet and Newman[11,12] and later modified by Zenyuk *et. al.*[13] and Lalit *et al.*[14] The model dimensions were adjusted to the measured cell parameters as shown in Table S2. The sintered Ti PTL properties were obtained by X-ray computed tomography.[15] First, the model was calibrated to the experimental polarization curve. Then, the mass-transport loss-free polarization curves were obtained by setting the reactant gas transport resistances in the CL and PTL to zero. The mass-transport overpotential was calculated by subtracting the mass-transport loss-free polarization curves from the original polarization curve.

Table S1. URFC RTEs comparison between this work and literature using comparable membranes. CG and CE stand for constant gas and constant electrode, respectively.

Temperature (°C) Charge/Discharge	Current density (A cm^{-2})	Operating modes	RTEs (%)	Membrane	Total Platinum Group metal loading (mg/cm^2)
80/80 (this work)	1.0	CE/CG	56/53	Nafion 212	1.3
80/80[16]	0.5	CG	50.3	Nafion 212	1.5
NA/NA[17]	0.1	CG	37.5	Nafion 212	0.5
65/65[18]	0.5	Discrete	40.6	Nafion 212	1.28
80/80[19]	0.5	CG	46	Nafion 212	0.8
75/75[20]	0.5	CG	49	Nafion 212	1.2
80/80[21]	0.4	CG	42	Nafion 212	0.7
75/70[22]	1.0	CG	43.8	Nafion 212	4.5
80/75[23]	0.5	CG	50.3	Nafion 212	1.5
80/80[24]	1.0	CE/CG	60/33	Nafion 212	1.3
80/80[25]	0.4	CG	49	Nafion 212	0.83

Table S2. Model dimensions and porosity, where ACL and CCL is anode and cathode catalyst layers, respectively.

	Membrane	ACL	CCL	GDL	PTL
Thickness (μm)	50.8	6	10	178	254
Porosity	0	0.6	0.36	0.8	0.36

Table S3. Round-trip efficiency comparison of the DBCCM at CE-URFC and CG-URFC modes under various current densities.

Current densities (A cm^{-2})	0.4	1.0	1.4	2.0
CE-URFC (H$_2$/O$_2$)	64.8	56.4	54.7	45
CE-URFC (H$_2$/Air)	62.4	52.5	46.5	36
CG-URFC (H$_2$/O$_2$)	64.6	53.6	46.8	35.2
CE-URFC (H$_2$/Air)	62.2	51.1	37.7	----

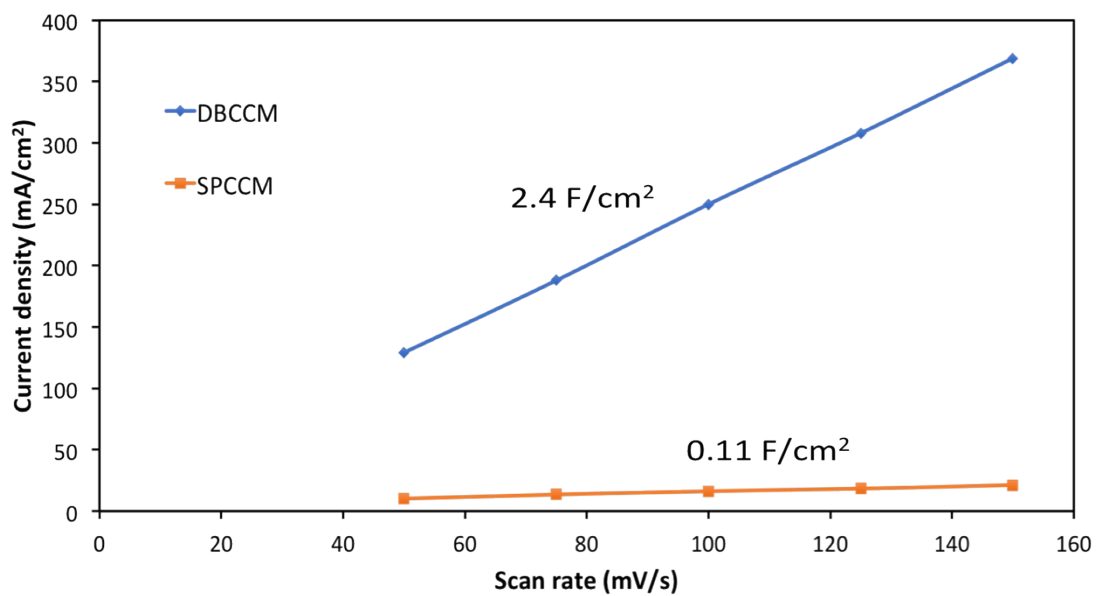The H$_2$/O$_2$ and H$_2$/Air indicate the oxidant during discharge.

Figure S1. The extracted Pt-Ir electrode double-layer capacitances (C_{dl}) of DBCCM and SPCCM, which are calculated based on cyclic voltammetry in the non-Faradaic region.
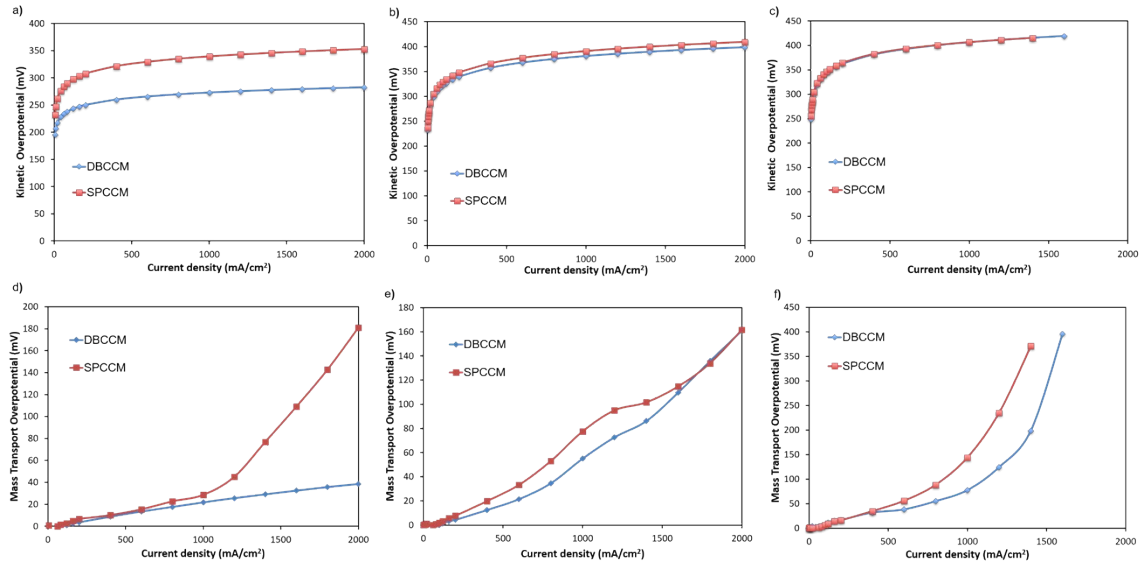
Figure S2. Kinetic overpotential comparison between DBCCM and SPCCM during CG-URFC operation: a) charge, b) discharge under O_2 feed o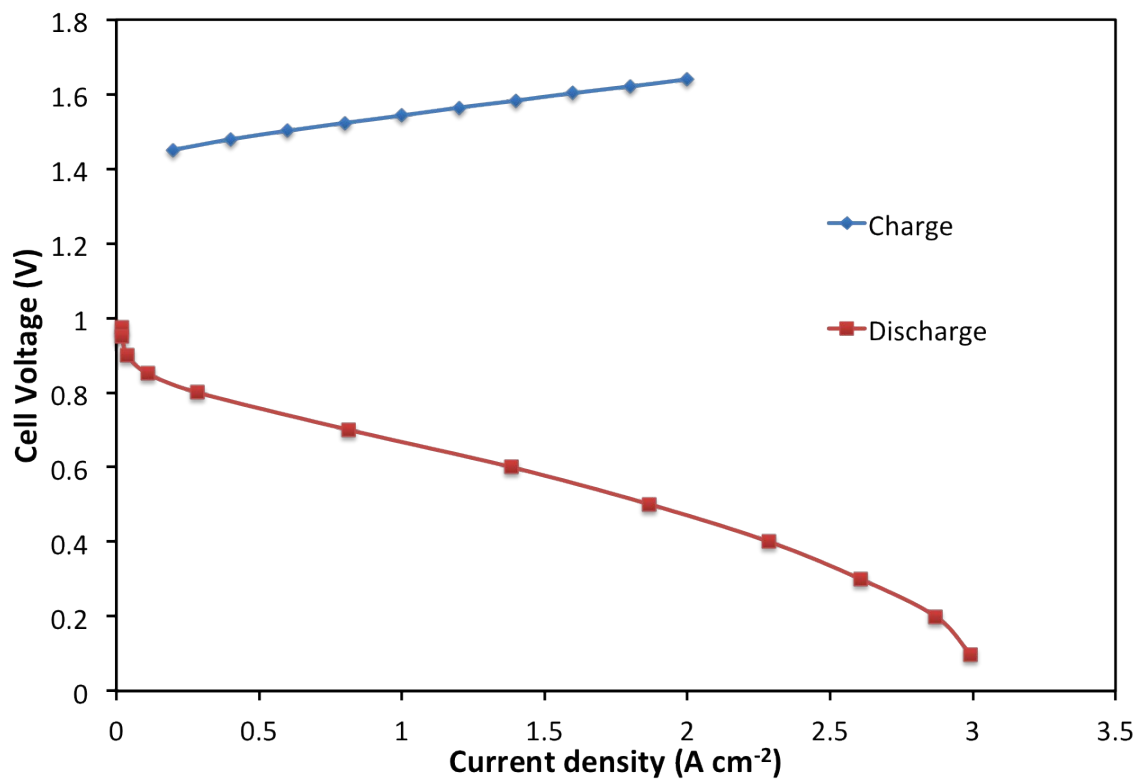n cathode, c) discharge under air feed on cathode; mass transport overpotential comparison between DBCCM and SPCCM during CG-URFC operation: d) charge, e) discharge under O_2 feed on cathode, f) discharge under air feed on cathode.

Figure S3. Charge and discharge cures of 25 cm² DBCCM at CG-URFC mode. The charging test was conducted at Proton Onsite Inc at 80 °C at ambient pressure. Discharging was conducted at Ballard Power Systems at 80 °C with H_2/Air feed.
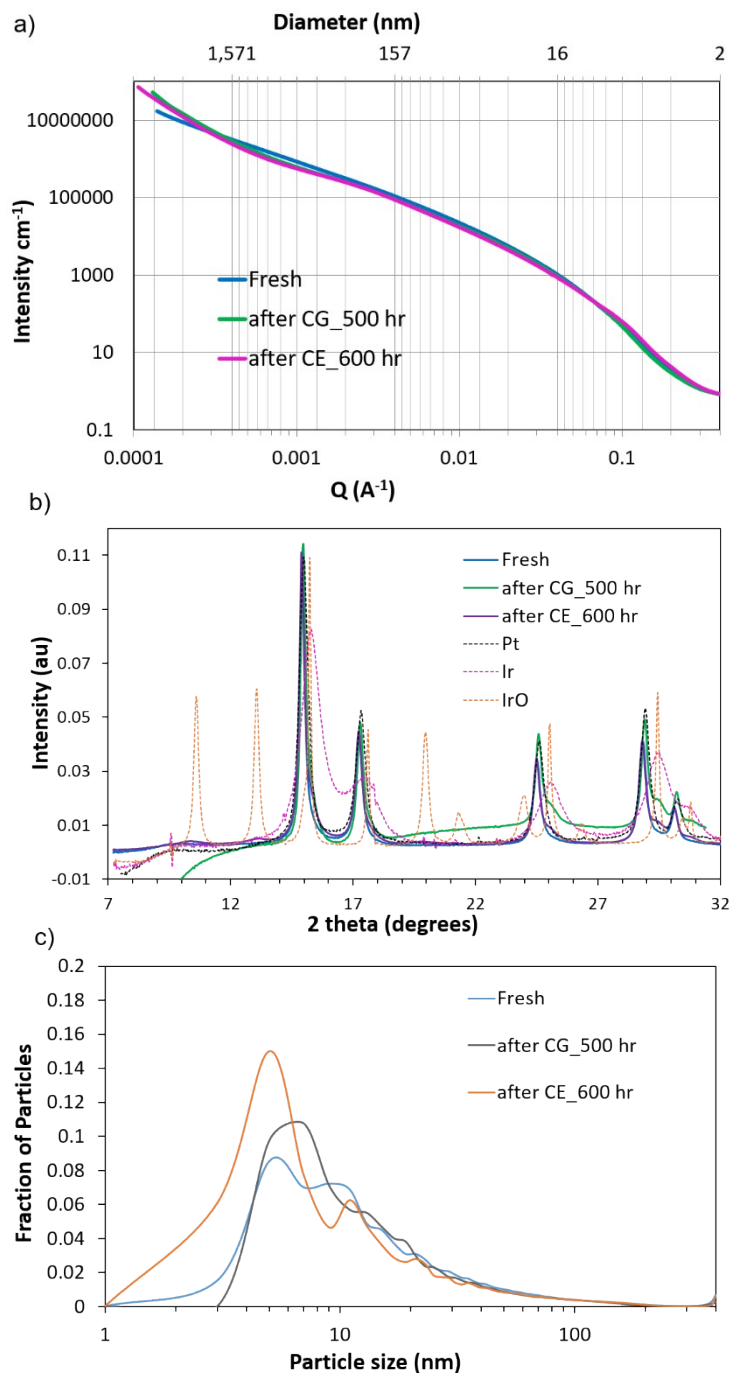
Figure S4. Fresh and post-durability of DBCCMs comparison of ultra-small-angle X-ray scattering: a) the scattered intensity (I(Q)) versus the scattering vector (Q), d) wide angle X-ray scattering patterns, c) volume fraction distribution. As comparison, the WAXS data shows similar diffraction patterns for the fresh and pos-durability CCMs, indicating the maintenance of crystal structures during the test. According to the USAXS data, there is slight volume fraction growth of small particles after both stability tests, with more growth after CE tests. This is likely due to the fact that CE-URFC operates at a wider voltage window than CG-URFC, which might lead to faster catalyst decay.
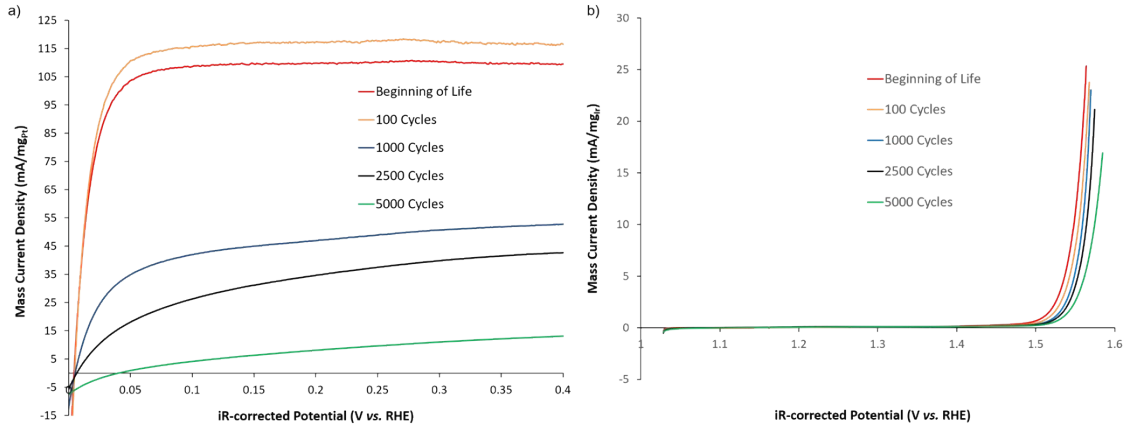
Figure S5. Polarization curves at different cycling stage during accelerated stress testing for a) hydrogen oxidation reaction using Pt black as catalyst, b) oxygen evolution reaction using Ir black as catalyst. The results indicate that during a typical CE-URFC anode potential working range between ~0.060V and 1.60 V (vs. RHE), the Pt catalyst degradation is more severe than Ir catalyst.
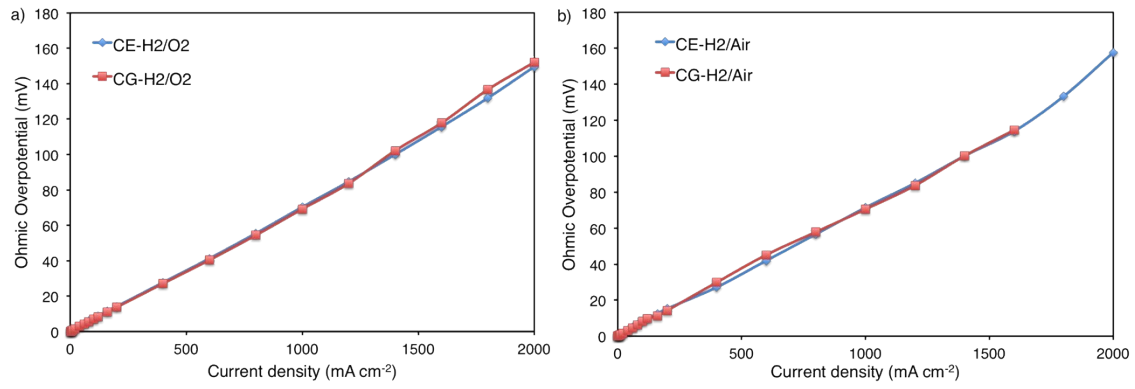
Figure S6. a), b) Ohmic overpotential comparison of DBCCM under CE and CG mode when oxygen and air are used as oxidant for fuel cell, respectively.
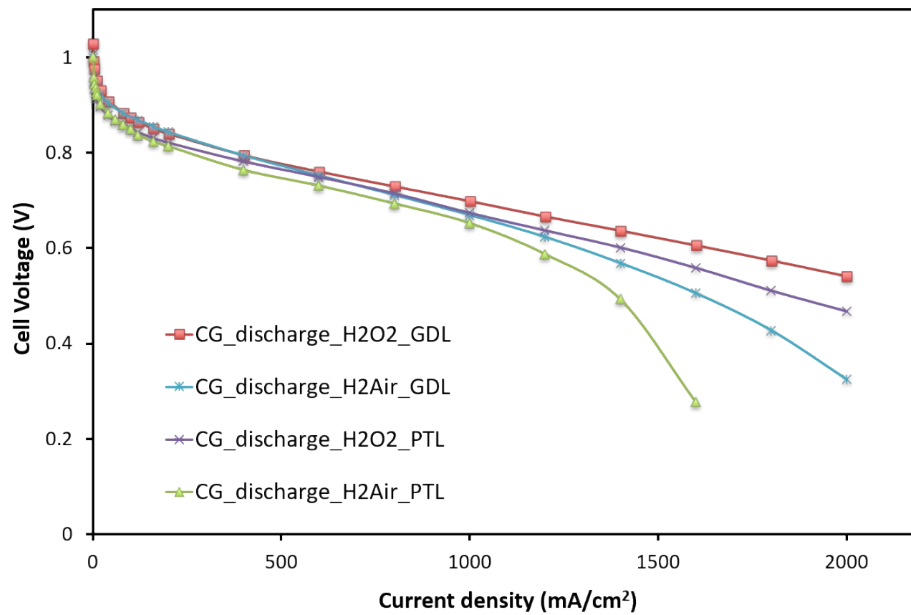
Figure S7. The comparison of discharge performance of DBCCM (Pt-Ir as cathode) under CG mode between using carbon-based gas diffusion layer (Sigracet 29BC) and porous transport layer (supplied by Nel Hydrogen/Proton Onsite).
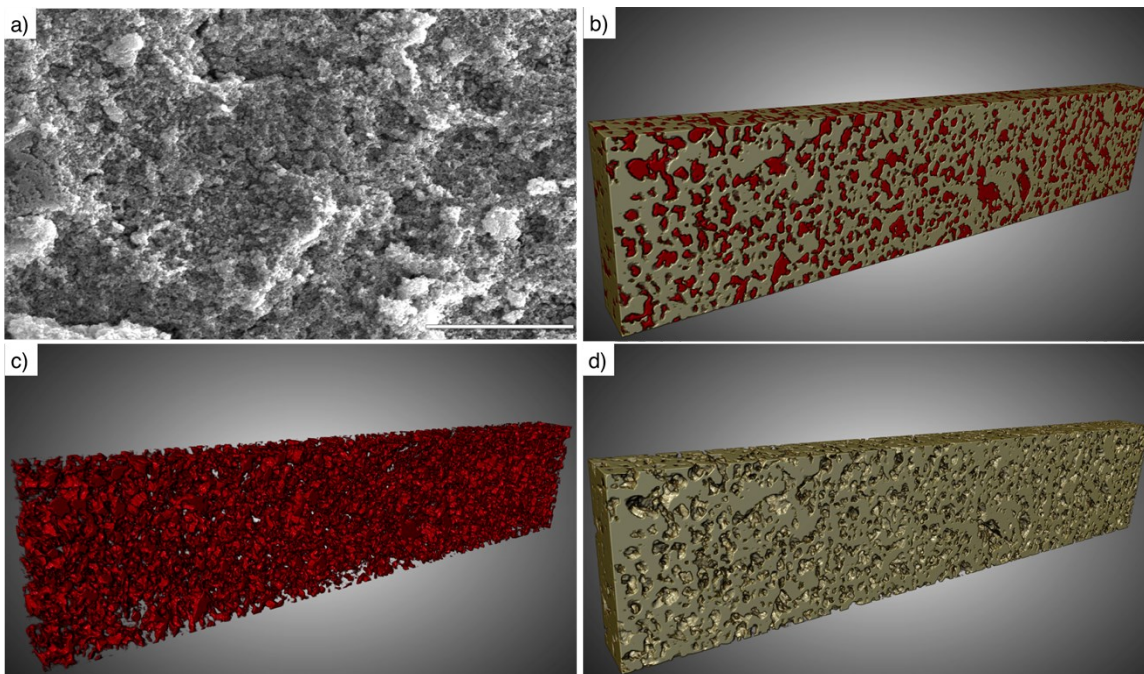
Figure S8. a) SEM image of the SPCCM, scale bar 5 μm, b) The reconstructed 3D Pt-Ir catalyst layer structure of SPCCM, c)-d) corresponded pore and solid 3D structures within the catalyst layer, respectively. The stack size is 11.73*2.51*0.86 μm. The total volume is 25.06 μm^3, total void volume is 7.34 μm^3.
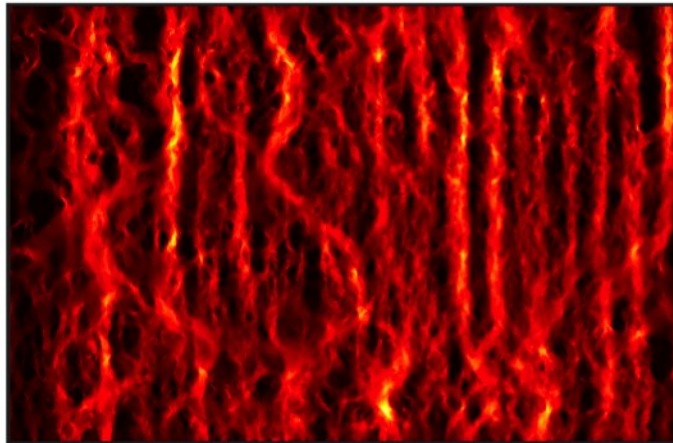
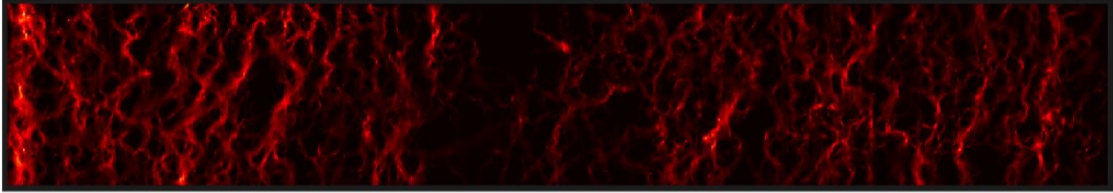Figure S9. Flux density of the DBCCM at transverse direction

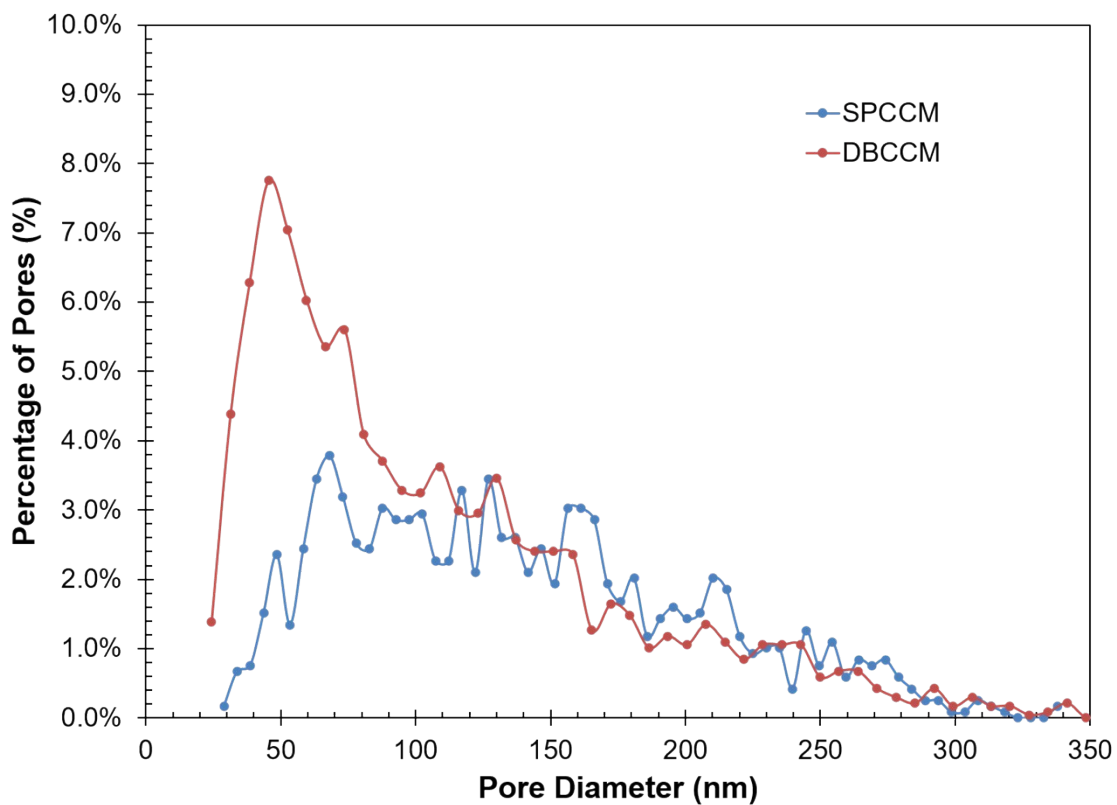Figure S10. Flux density of the SPCCM at transverse direction

Figure S11. Pt-Ir electrode pore size distribution comparison between the doctor bladed catalyst coated membrane (DBCCM) and spray coated catalyst coated membrane (SPCCM).
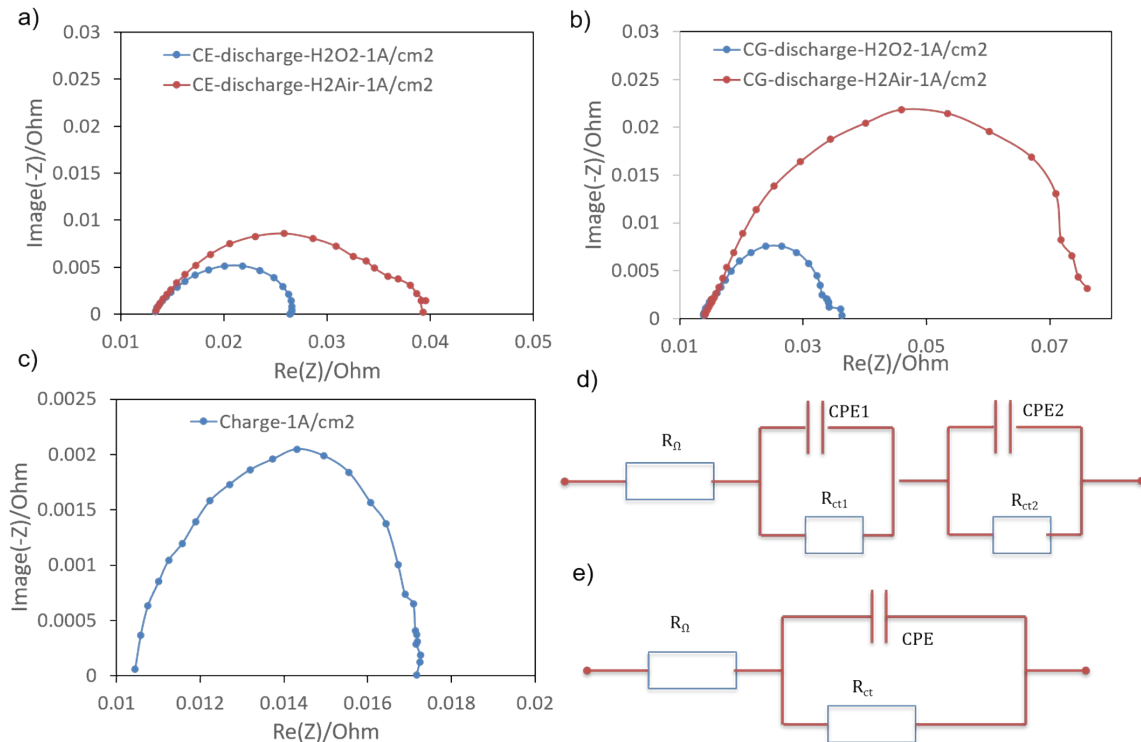
Figure S12. Nyquist plots at current density of 1 A cm^{-2}: a) discharge with H$_2$/O$_2$ and H$_2$/Air feed under CE-URFC mode, b) discharge with H$_2$/O$_2$ and H$_2$/Air feed under CG-URFC mode, c) charging, d)-e) the two equivalent circuits of URFC for discharging and charging, respectively. The results show that during discharging under both CE and CG modes, a distortion of the kinetic loop was observed, resulting in two semicircles, which corresponds to the equivalent circle of Figure S10d; during charging, a single semicircle loop was observed, indicating that the oxygen evolution reaction kinetics dominated the electrode behavior at this current density.

Reference:

1. Arganda-carreras, I. *et al.* Trainable Weka Segmentation : a machine learning tool for microscopy pixel classification. *Bioimage informatics* **33**, 2424–2426 (2017).
2. Gostick, J. *et al.* OpenPNM: A Pore Network Modeling Package. *Comput. Sci. Eng.* (2016).
3. Cooper, S. J., Bertei, A., Shearing, P. R., Kilner, J. A. & Brandon, N. P. TauFactor : An open-source application for calculating tortuosity factors from tomographic data. *SoftwareX* **5**, 203–210 (2016).
4. Ito, H., Abe, K., Ishida, M. & Min, C. Effect of through-plane polytetrafluoroethylene distribution in a gas diffusion layer on a polymer electrolyte unitized reversible fuel cell. *Int. J. Hydrogen Energy* **40**, 16556–16565 (2015).
5. Jemianlt, P. R., Weertman, J. R. & Long, G. G. CHARACTERIZATION OF 9Cr-IMoVNb STEEL BY ANOMALOUS SMALL-ANGLE X-RAY SCATTERING. *Acta Met. mater* **39**, 2477–2487 (1991).
6. Ilavsky, J. *et al.* Ultra-small-angle X-ray scattering at the Advanced Photon Source. *J. Appl. Crystallogr.* **42**, 469–479 (2009).
7. Ilavsky, J. Nika : software for two-dimensional data reduction. *J. Appl. Crystallogr.* **45**, 324–328 (2012).
8. Ilavsky, J. & Jemian, P. R. Irena : tool suite for modeling and analysis of small-angle scattering. *J. Appl. Crystallogr.* **42**, 347–353 (2009).
9. Bratsch, S. G. Standard Electrode Potentials and Temperature Coefficients in Water at 298.15 K. *J. Phys. Chem. Ref. Data* (1989) doi:10.1063/1.555839.
10. Harrison, K. W., Remick, R., Martin, G. D. & Hoskin, A. *Hydrogen Production : Fundamentals and Case Study Summaries Summaries*. (2010).
11. Balliet, R. J. Modeling Cold Start in a Polymer-Electrolyte Fuel Cell. (2010).
12. Balliet, R. J., Newman, J. & Soc, J. E. Cold Start of a Polymer-Electrolyte Fuel Cell I . Development of a Two- Dimensional Model. *J. Electrochem. Soc.* **8**, B927–B938 (2011).
13. Zenyuk, I. V, Soc, J. E., Zenyuk, I. V, Das, P. K. & Weber, A. Z. Understanding Impacts of Catalyst-Layer Thickness on Fuel-Cell Performance via Mathematical Modeling Understanding Impacts of Catalyst-Layer Thickness on Fuel-Cell Performance via Mathematical Modeling. *J. Electrochem. Soc.* **7**, F691–F703 (2016).
14. Pant, L. M. *et al.* Along-the-channel modeling and analysis of PEFCs at low stoichiometry: Development of a 1 + 2D model. *Electrochim. Acta* 134963 (2019) doi:10.1016/j.electacta.2019.134963.
15. Leonard, E. *et al.* Interfacial analysis of a PEM electrolyzer using X-ray computed tomography. *Sustain. Energy Fuels* 921–931 (2020) doi:10.1039/c9se00364a.
16. Huang, S., Ganesan, P., Jung, H. & Popov, B. N. Development of supported bifunctional oxygen electrocatalysts and corrosion-resistant gas diffusion layer for unitized regenerative fuel cell applications. *J. Power Sources* **198**, 23–29 (2012).
17. Pai, Y. & Tseng, C. Preparation and characterization of bifunctional graphitized carbon-supported Pt composite electrode for unitized regenerative fuel cell. *J.*

Power Sources **202**, 28–34 (2012).

18. Zhuo, X., Sui, S. & Zhang, J. Electrode structure optimization combined with water feeding modes for Bi-Functional Unitized Regenerative Fuel Cells. *Int. J. Hydrogen Energy* **38**, 4792–4797 (2013).

19. Lee, B. *et al.* Electrochemistry Communications Development of porous Pt/IrO2/ carbon paper electrocatalysts with enhanced mass transport as oxygen electrodes in unitized regenerative fuel cells. *Electrochem. commun.* **64**, 14–17 (2016).

20. Eun, J., Karuppannan, M., Joong, O. & Cho, Y. Development of high-performance membrane-electrode assembly in unitized regenerative fuel cells. *J. Ind. Eng. Chem.* **80**, 527–534 (2019).

21. Choe, S., Lee, B. & Jang, J. H. Effects of Diffusion Layer (DL) and ORR Catalyst (ORR) on the Performance of M ORR/IrO2/DL Electrodes for PEM-Type Unitized Regenerative Fuel Cells. *J. Electrochem. Sci. Technol.* **8**, 7–14 (2017).

22. Sadhasivam, T. *et al.* A comprehensive review on unitized regenerative fuel cells: Crucial challenges and developments. *Int. J. Hydrogen Energy* 1–19 (2016) doi:10.1016/j.ijhydene.2016.10.140.

23. Huang, S. ., Ganesan, P., Jung, W. S., Cadirov, N. & Popov, B. N. Development of Supported Bifunctional Oxygen Electrocatalysts with High Performance for Unitized Regenerative Fuel Cell Applications. *ECS Trans.* **33**, 1979–1987 (2010).

24. Regmi, Y. N. *et al.* A low temperature unitized regenerative fuel cell realizing 60% round trip efficiency and 10 000 cycles of durability for energy storage applications. *Energy Environ. Sci.* 2096–2105 (2020) doi:10.1039/c9ee03626a.

25. Lim, A. *et al.* Low-loading IrO2 supported on Pt for catalysis of PEM water electrolysis and regenerative fuel cells. *Appl. Catal. B Environ.* **272**, 118955 (2020).